Carbon Dioxide Capture by Modified UVM-7 Adsorbent

Fatemeh Babaie[1], Seyed Hamed Mousavi[*1], Ali Mohammadalizadeh[2, 3], Nastaran Hazrati[4]

[1]Faculty of Caspian, College of Engineering, University of Tehran, Guilan, Iran.
[2]Gas Research Division, Research Institute of Petroleum Industry (RIPI), Tehran, Iran.
[3]Department of Chemical Engineering, Polytechnique Montreal, Montréal, Québec, Canada.
[4]Faculty of Chemistry, Amirkabir University of Technology, Tehran, Iran.

(Received 8 January 2014, Accepted 22 July 2014)

Abstract

In this study, bimodal meso-porous silica (UVM-7) synthesized and fabricated amino silane modified supports were characterized by powder X-ray diffraction (XRD), N_2 adsorption/desorption, transmission electron microscope (TEM), elemental analysis and titration. Capacity of CO_2 capture on modified bimodal pore structure silica at 70° C was calculated using breakthrough curves; and it was found that the modified UVM-7 captured more CO_2 than unmodified UVM-7 and pore structure of UVM-7 make it suitable for loading large molecules such as tri-amino silanes. The adsorbents modified with tri-amino silane showed the largest capacity. Dynamic and kinetic of adsorption were investigated by mathematical models in order to prediction of adsorption behavior. Yoon Nelson model was successfully employed to describe the adsorption breakthrough curves of CO_2 and Avrami model applied as a kinetic model and was in good agreement with experimental data in comparison with two other kinetic models including Lagergen's pseudo-first and pseudo-second order models.

Keywords: CO_2**,** Adsorption Isotherm, Breakthrough, Carbon Capture, Flue Gas

Introduction

Emission of CO_2 has ever been of serious concern to developed countries in terms of global warming in recent decade. CO_2 is considered as one of the most important anthropogenic greenhouse gases as approximately 7Gt of carbon is emitted to the earth's atmosphere each year [1-4]. Acting as a trap for heat received from the sun, increasing level of CO_2 in atmosphere results in arising in global mean temperature. Carbon capture and sequestration (CCS) is an important part of global carbon dioxide reduction program and many researches, therefore, have focused their attention on establishment of a robust technology to capture CO_2 from various sources emitting this key greenhouse gas [5-8].

Flue gases resulted from post-combustion in fossil fuel-burning power plants are one of the concentrated sources of CO_2 containing between 5 and 15 volume percentage of carbon dioxide. Existing power plants could be retrofitted for post-combustion CO_2 capture and purification using known and developing separation techniques [9]. Technologies such as pre-combustion CO_2 capture from power generation point sources that use fossil fuels are also of particular interest [10].

Using solid sorbents have been one of the most promising solutions to the problem of post combustion carbon dioxide emission in recent years [2, 3].

Among various methods for post-combustion carbon dioxide capture, adsorption is object of attention from its low energy requirement point of view therefore many efforts have been made to develop high efficient adsorbents with the aim of CO_2 capture of flue gas [11-12].

In this area, amine-functionalized carbon-based materials and silica-based materials are two kinds of sorbents under consideration [13].

Corresponding author: Tel: +98 1824653267 Fax: +98 1824652600 Email: mhmousavi@ut.ac.ir

MCM-41(Mobil Composition of Matter -41) and SBA-15(Santa Barbara Amorphous-15) meso-porous adsorbents are commonly chosen as support because of the their large well-defined pore channel and pore volumes which allow easy access of amine molecules into the structure so that significant quantities of amine can be loaded onto the adsorbent [14].

In this study UVM-7 as bimodal pore silica based material was synthesized and subsequently functionalized with three types of amino silanes via grafting method. Then capacity of the absorbents and kinetic of adsorption were investigated and mathematical models accuracy was verified.

With the intention of comparing the results of synthesized adsorbents with commercial ones, CO_2 adsorption on 13x has been examined.

Materials and methods

Synthesis and functionalizing of UVM-7

The atrane route is the most common way to synthesize UVM-7 [15]. In a typical synthesis, TEOS (tetraethyl ortho silicate) was added to predetermined amounts of TEAH3 (tri ethanol amine) and the solution was heated up to 140 °C. After cooling down to 90 °C, CTAB (cetyl tri methyl ammonium bromide) was added to the solution. Hereafter, water was added slowly to this solution under stirring until a white suspension appeared and then the suspension was left for 4 hours at room temperature. The solid was filtered, washed with sufficient amount of water and acetone and dried in oven at 80 °C overnight. Thermo calcination of as-synthesized UVM-7 was carried out under flow of air up to 550 °C for 6 hours. The final molar composition of reactants was 1.0 TEOS: 3.5 TEAH3: 0.25 CTAB: 90 H2O.All chemicals were supplied by Merck and Sigma-Aldrich companies.

For functionalization of UVM-7 with amine groups, predetermined amounts of $C_9H_{23}NO_3Si$, $C_8H_{22}N_2O_3Si$ and $C_{10}H_{27}N_3O_3Si$ to get 5 wt % of organosilane/UVM-7 and 2g of UVM-7 was added to appropriate amount of toluene and stirred for 6 h at 80 °C, followed by filtering and washing with proper amounts of ethanol and water. Three amine-functionalized UVM-7 materials were dried at 80 °C overnight. The final samples were denoted as $x\%N^y$-U, where U, x and N^y indicate UVM-7, aminosilane loading and the type of aminosilne as N^1= ($C_9H_{23}NO_3Si$), N^2= ($C_8H_{22}N_2O_3Si$) and N^3= ($C_{10}H_{27}N_3O_3Si$) respectively.

Samples characterization

X-ray diffraction (XRD) patterns were recorded on a Seifert TT 3000 diffract meter using with nickel filtered Cu Kα radiation of wavelength 0.15405 nm. Physisorption of Nitrogen was measured at 77 K using a BEL-SORP-mini porosimeter. Surface area, pore size and volume values were calculated from nitrogen adsorption–desorption isotherms. Prior to analysis, the samples were out gassed in vacuum for 4 h at 363 K until a stable vacuum of 0.1 Pa was reached.

Pore size distribution was calculated using the Barrett-Joyner-Halenda (BJH) method. Titration of three amine-functionalized UVM-7 materials was carried out using 0.05 molar ethanolic solution of hydrochloric acid using METTLER TOLEDO G20 apparatus.

Elemental analysis was performed using PerkinElmer 2400 (Series II) CHN elemental analyzer for determination of nitrogen residue of parent, and three amine-functionalized UVM-7 materials. The high resolution TEM images of the sorbents were recorded on a Philips CM30 with LaB6 electron gun at 250 kV. Before TEM characterization samples were dispersed in ethanol solution and deposited on the grids made of copper.

Experimental set-up

Figure 1 shows a schematic diagram of prepared set-up to examine the CO_2 adsorption capacity. 0.25g of each sample

with 100 mesh particle size were loaded in a U tube reactor.

The breakthrough curves of CO_2 adsorption was obtained by analyzing the effluent gas mixture using a gas chromatograph (SHIMADZU, model: NO.507886 GC-4C PTF) equipped with thermal conductivity detector.

With the aim of comparing the results with literature [16], CO_2 adsorption was examined at 70 °C. Each sample was degassed using Argon at 120 °C for 1hr before adsorption test.

Dynamic adsorption of CO_2

The dynamic adsorption capacity was considered using the breakthrough curves according to equation (1):

$$q = \frac{FC_0t_q}{W} \quad (1)$$

Where q is CO_2 adsorption capacity, F is the total molar flow, C_0 is the concentration of the CO_2 in the feed stream, W is the amount of the adsorbent loaded in the adsorption bed. The time t_q is estimated by Equation (2) [17]:

$$t_q = \int_0^{\infty} (1 - \frac{C_A}{C_0})\, dt \quad (2)$$

Where, C_A and C_0 are the outlet and inlet concentration of the stream through the fixed bed, respectively.

Kinetic of adsorption

Fast adsorption kinetics is one of the most important properties expected from a superior adsorbent. In this study, three different kinetic models including lagergren's pseudo-first order, pseudo-second order and Avrami's kinetic model presented by equations (3), (4) and (5) respectively were investigated:

$$\frac{dq_t}{dt} = k_f(q_e - q_t) \quad (3)$$

$$\frac{dq_t}{dt} = k_s(q_e - q_t)^2 \quad (4)$$

$$\frac{dq_t}{dt} = k_A^n t^{n-1}(q_e - q_t \quad (5)$$

Where t is the time elapsed from the beginning of the adsorption process, q_e and q_t are the adsorption capacity at equilibrium and at a given point in time, respectively. k_f, k_s and k_A are the kinetic constants for pseudo-first order, pseudo-second order and Avrami's kinetic model, respectively. After integration and applying the boundary conditions (q_t=0, t=0 and q_t=q_e, t=∞) the integrated forms of the Equations (3) to (5) become as follows [17]:

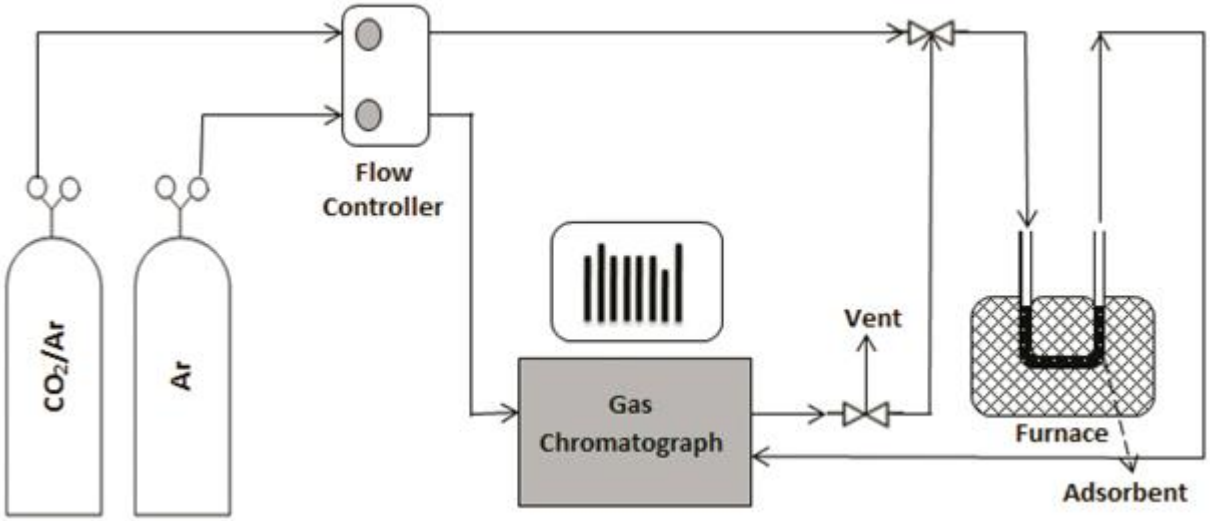

Figure.1: Schematic diagram of experimental set-up

$$q_t = q_e[1 - \exp(-k_f t)] \quad (6)$$

$$q_t = \frac{k_s q_e^2 t}{1 + q_e k_s t} \quad (7)$$

$$q_t = q_e[1 - \exp(-(k_A t)^{n_A})] \quad (8)$$

Results and Discussions

XRD analysis

XRD patterns of all samples, i.e. UVM-7, 5%N[1]-U, 5%N[2]-U and 5%N[3]-U are shown in Figure 2*a-d*, respectively.

A strong diffraction peak is observed in all XRD patterns, which is characteristic of this type of meso/macros porous material. However, this strong peak attributed to diffraction from d_{100} plane is accompanied with a broad diffraction peak at higher angles in all four samples. These broad peaks might be assigned to d_{110} and overlap of d_{200} and d_{210} diffraction peaks based on hexagonal symmetry. As the peak become broader and weaker, the structural order of pores decreases.

This observation might be an indication of low-ordered intra-nanoparticle mesopores system (small pores) in samples caused by grafting of different type of amine groups on UVM-7 support. As the number of amine groups in the grafted organosilane increases (Figure 2*b-d*, respectively), the broadness as well as the weakness of all diffraction peaks including d_{100}, d_{110}, d_{200} and d_{210} enhance.

The aforementioned observations may be interpreted as a decrease in structural order of the corresponding sample. Presence of secondary large pore system in the border between meso and macrospores without long-range order could be determined using nitrogen physicsorption experiment.

N_2 adsorption

Textural properties of synthesized sample were investigated by nitrogen physisorption. Figure 3a-d illustrates the nitrogen isotherms of UVM-7, 5%N[1]-U, 5%N[2]-U and 5%N[3]-U, respectively. The corresponding isotherm of samples displays two distinct regions at medium and high relative pressure which might be attributed to the presence of bimodal pore system. The inflection of type IV isotherm at medium relative pressure is typical of mesoporous materials (as defined by IUPAC) and suggests a well-ordered array of small mesopores in all samples [18].

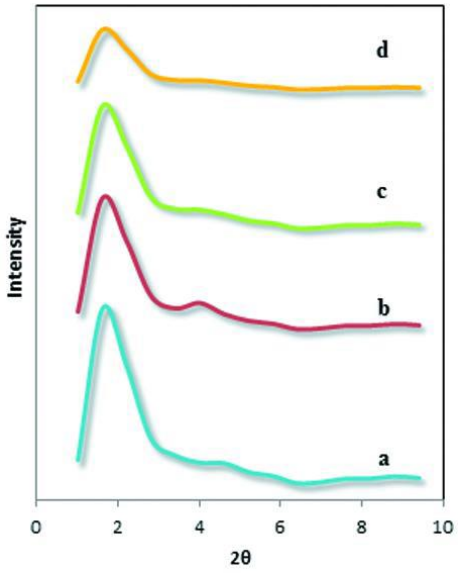

Figure 2: X-ray diffraction patterns of a) UVM-7 b) 5%N1-U c) 5%N2-U d) 5%N3-U

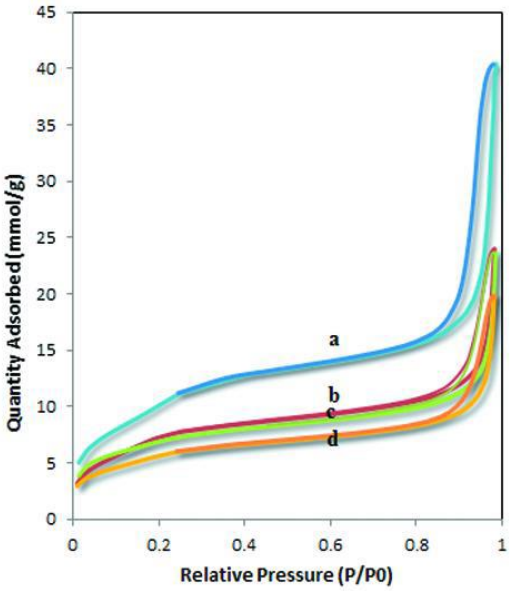

Figure 3: Nitrogen adsorption/desorption isotherms of a) UVM-7 b) 5%N1-U c) 5%N2-U d) 5%N3-

Table 1: Textural properties of amine-grafted UVM-7 samples

Sample	a_0 (nm)	S_{BET} ($m^2\ g^{-1}$)	Pore size (nm)		Pore Volume ($cm^3\ g^{-1}$)		Pore wall (nm)
			Small	Large	Small	Large	
UVM-7	5.59	863	2.67	52.2	0.42	0.84	2.92
5%N^1-U	5.59	626	2.62	42.2	0.27	0.41	2.97
5%N^2-U	5.59	567	2.64	41.5	0.25	0.39	2.99
5%N^3-U	5.59	466	2.59	42.1	0.20	0.35	3.04

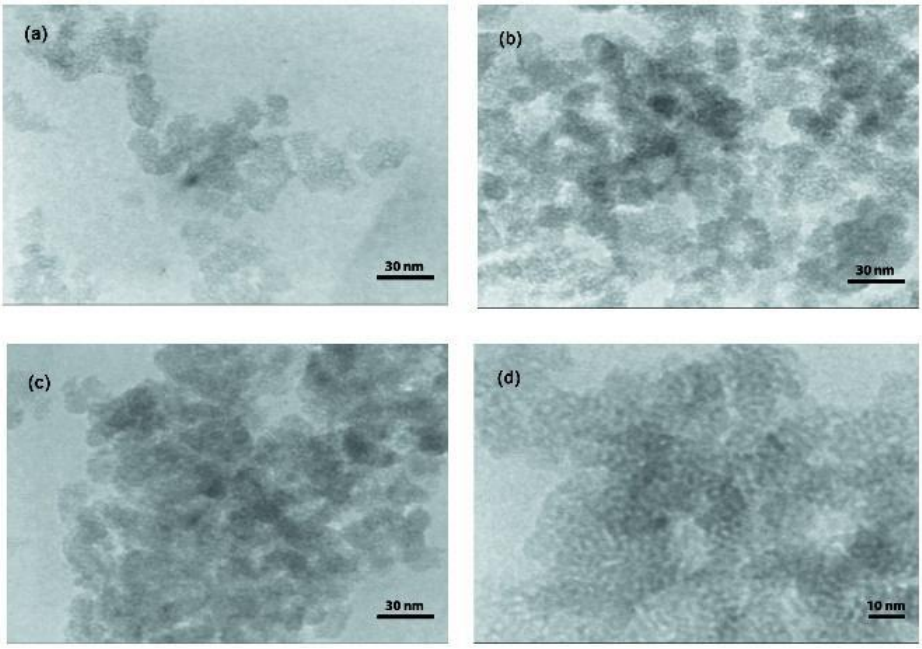

Figure 4: TEM images of (a) UVM-7 (b) 5%N1-U (c) 5%N2-U (d) 5%N3-U

This behaviour can be explained by fully reversible capillary condensation/ evaporation of nitrogen at this step. However, after functionalization of UVM-7, the sharpness of this region remarkably decreases (Figure 3b-d). The second region observed in all four isotherms (Figure 3a-d) at relative pressure near 1 is a region with very sharp inflection in gas uptake, which could be due to the filling of secondary large mesopores with condensed nitrogen.

These two distinct regions in all samples confirm that the UVM-7 bimodal pore system remained unchanged after the functionalization with different type of amine groups. In amine-functionalized samples (Figure 3b-d) the amounts of gas uptake in these two regions decreased in the following order: 5%N^1-U>5%N2-U>5%N^3-U. As the larger the size of amine chain, the higher the volume in the corresponding sample

occupied. Textural properties of all four samples are given in Table 1.

It can be deduced from volume of small and large mesopores of four synthesized samples in Table 1 that amine functional groups have been grafted inside both small and large mesopores but the contribution of latter is to a greater extent than former. Furthermore, decrease of pore size of large mesopores is predominant with respect to small mesopores in 5%N^1-U, 5%N^2-U and 5%N3-U. This observation supports the assumption of grafting of amine functional groups mainly inside the large mesopores.

Titration

The obtained results of acid/base titrations imply that up to 90 % of three organo silanes were grafted on silica walls of corresponding sample.

Elemental analysis

Elemental analysis provides further evidence for amine functional groups grafted on the 5%N^1-U, 5%N^2-U and 5%N^3-U. The yield of functionalization can be calculated using elemental analysis results in which ratio of nitrogen content of three amine-functionalized samples is divided by the amount of nitrogen of three amino-organosilanes used for functionalization. The results indicate that at least 95 % of amino-organosilanes were grafted on the silica wall of corresponding sample.

TEM analysis

In practice, characteristic architecture of the bimodal porous silicas can be appreciated by means of electron microscopy techniques. The high resolution TEM images of the UVM-7porous silica and modified samples are shown in Figure 4. As it can be seen, there are no significant differences among the raw UVM-7 and functionalized samples.

Breakthrough Curves

Figure 5 illustrates the CO_2 adsorption breakthrough curves of UVM samples. For all aminated samples, the shapes of the adsorption curves are similar. So they depict similar adsorption behaviour. Breakthrough times of CO_2 adsorption were in the order as 5%N^3-U>5%N^2-U>5%N^1-U>U. Thus, tri aminosilane was found the best functional group with high adsorption capacity.

The break times and calculated capacities are shown in Table 2. Comparing with commercial adsorbents such as zeolite 13X, functionalized UVM adsorbents shows better adsorption capacities and break times. In actual applications, the adsorption columns are regenerated before breakthrough, so the breakthrough time and the corresponding uptake can be used as a standard for evaluating the adsorption ability of an adsorbent. Tri-aminosilane has more activated sites to adsorb CO_2 than other aminosilanes and large pore size of UVM-7 decrease inaccessibility of large molecules of tri-aminosilane. The total number of amines present does not directly describe the adsorbent's equilibrium CO_2 capacity or uptake kinetics. When preparing adsorbents via silane chemistry, it is essential to maximize both their amine loadings and amine efficiencies.

Amine efficiency, defined here as the number of captured moles of CO_2 per mass unit divided by the moles of N per mass unit, gives a reflection of the adsorbent efficacy in perspective with its potential. Amine efficiencies less than 0.5 for anhydrous conditions and 1.0 for humid conditions reflect either amine inaccessibility or non-ideal adsorption operating conditions [3].

As shown in Table 2 amine efficiencies for aminated samples are larger than 0.5 that it may be a result of both chemisorption and physisorption.

Modeling of breakthrough curves

To model CO_2 adsorption on these adsorbents, Yoon and Nelson model was used to simulate the breakthrough curves according to the Equation (9) [19]:

$$\frac{C_A}{C_0} = \frac{1}{1 + \exp(K(\tau - t))} \quad (9)$$

Where, K is the Yoon-Nelson constant that depends on the diffusion characteristics of the mass transfer zone, τ is the stoichiometric time (time for CA = 0.5 C0), CA is concentration of CO_2 in the effluent and C0 is initial concentration of CO_2. Equation (9) has been fitted to experimental results for breakthrough curves, values of τ and the Yoon-Nelson constant (K) have been calculated (Table3). The modeled curve has been obtained and shown by line in breakthrough curves (figure 6).

The modeled curve shows excellent agreement with the experiments. Higher rate constant for raw UVM-7 in table 3 indicates higher speed of CO_2 adsorption by UVM-7. The $5N^3$-U has the lowest K (0.7858 min-1) and the largest τ (8.955 min), being consistent with its highest dynamic CO_2 adsorption capacity (1.344 mmol.g-1).

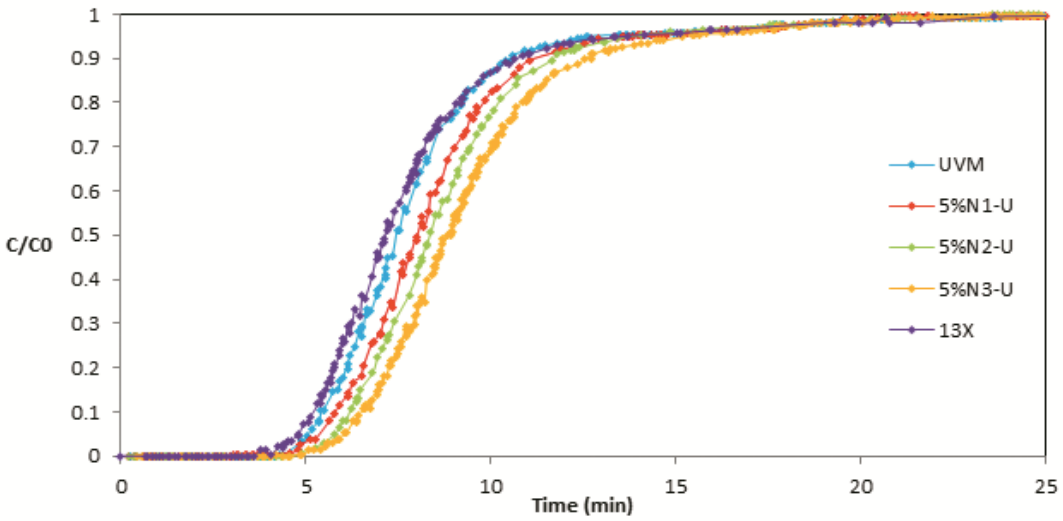

Figure 5: Breakthrough curves of (a) UVM-7, (b) 5%N1-U, (c) 5%N2-U and (d) 5%N3-

Table 2: The amine content and the adsorption properties of the adsorbents

Sample Name	Break Time (min)	CO_2 Adsorption Capacity (mmol/g)	Amine Content (mmol/g)	N content (mmol/g)	Amine efficiency (mol CO_2/mol N)
13X	4.926	1.142	0	0	-
UVM-7	5.038	1.147	0	0	-
5%N^1-U	5.400	1.216	0.7345	0.7345	1.655
5%N^2-U	5.762	1.262	0.7340	1.4680	0.860
5%N^3-U	6.042	1.344	0.7115	2.1345	0.630

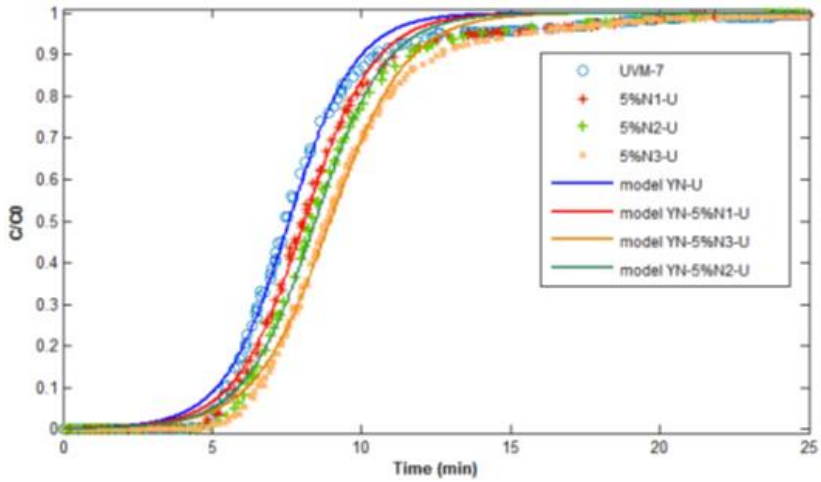

Figure 6: Modeling of breakthrough curves of (a)UVM-7, (b)5%N1-U, (c)5%N2-U and (d) 5%N3-U

Table 3: Values of the Yoon Nelson modelparameters for CO_2 adsorption

Sample	Parameters		Goodness of fit	
	τ(min)	k (min^{-1})	R-Square	SSE
UVM-7	7.577	0.9041	0.9971	0.1177
5%N^1-U	8.089	0.8604	0.9975	0.08366
5%N^2-U	8.458	0.8494	0.9976	0.05193
5%N^3-U	8.955	0.7858	0.997	0.1479

Kinetic modeling

Figure 7(a-b) depicts the CO_2 uptake curves as a function of adsorption time for raw UVM-7 and functionalized samples moreover the corresponding adsorption behaviors predicted by different kinetic models. Typically, most of adsorption (>90% of equilibrium capacity) took place during the first 6-7 minutes of CO_2 exposure, afterwards the rate of adsorption became much slower until complete CO_2 saturation. The overall kinetics of CO_2 adsorption on a functionalized solid sorbent is influenced by the intrinsic reaction kinetics of CO_2 with the functional group present, as well as the mass transfer or diffusion resistance of the gas phase through the sorbent structures.

The porous support structures of functionalized solid sorbents also can be tailored, to minimize the diffusion resistance. The faster an adsorbent adsorbs and desorbs CO_2, the less content of it will be needed to capture a given volume of flue gas [20]. As seen in Table 4, the predicted equilibrium capacity (qe) by Avrami model is in all cases closer to the experimental data. Also pseudo-first model shows better results than pseudo-second model.

Comparing the value of Yoon Nelson K parameter and the k parameters obtained from these kinetic models, it can be concluded that these parameters are not rate constant, but rather are a complex function involving different parameters such as the kinetic constant for desorption, the surface coverage at equilibrium and the change of adsorbate concentration during the process.

For example, Azizian et al. [21] demonstrated that the value of k obtained from the pseudo-second order kinetic model is not the kinetic constant for adsorption in a strict sense. In a similar manner, the fractional order in the Avrami model suggests that the value of kA is an overall constant representing various reaction steps [17].

Table 4: Values of the kinetic model parameters for CO_2 adsorption on UVM-7 and modified samples

	Parameters	UVM-7	5%N1-U	5%N2-U	5%N3-U
Avrami model	k_a (min^{-1})	0.2069	0.1974	0.1912	0.1768
	q_e ($mmol.g^{-1}$)	1.144	1.214	1.267	1.342
	n	1.391	1.405	1.394	1.454
	R^2	0.9979	0.998	0.9975	0.9975
Pseudo-first	k_f (min^{-1})	0.2067	0.1917	0.181	0.1803
	q_e ($mmol.g^{-1}$)	1.162	1.246	1.326	1.381
	R^2	0.9814	0.9805	0.9792	0.9711
Pseudo-second	k_s ($g\ mmol^{-1}\ min^{-1}$)	0.1881	0.1395	0.1056	0.1253
	q_e ($mmol.g^{-1}$)	1.343	1.5	1.677	1.651
	R^2	0.9416	0.9491	0.9535	0.927

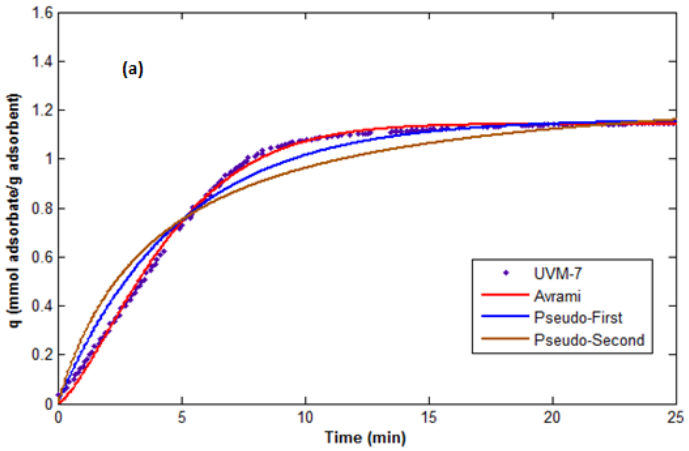

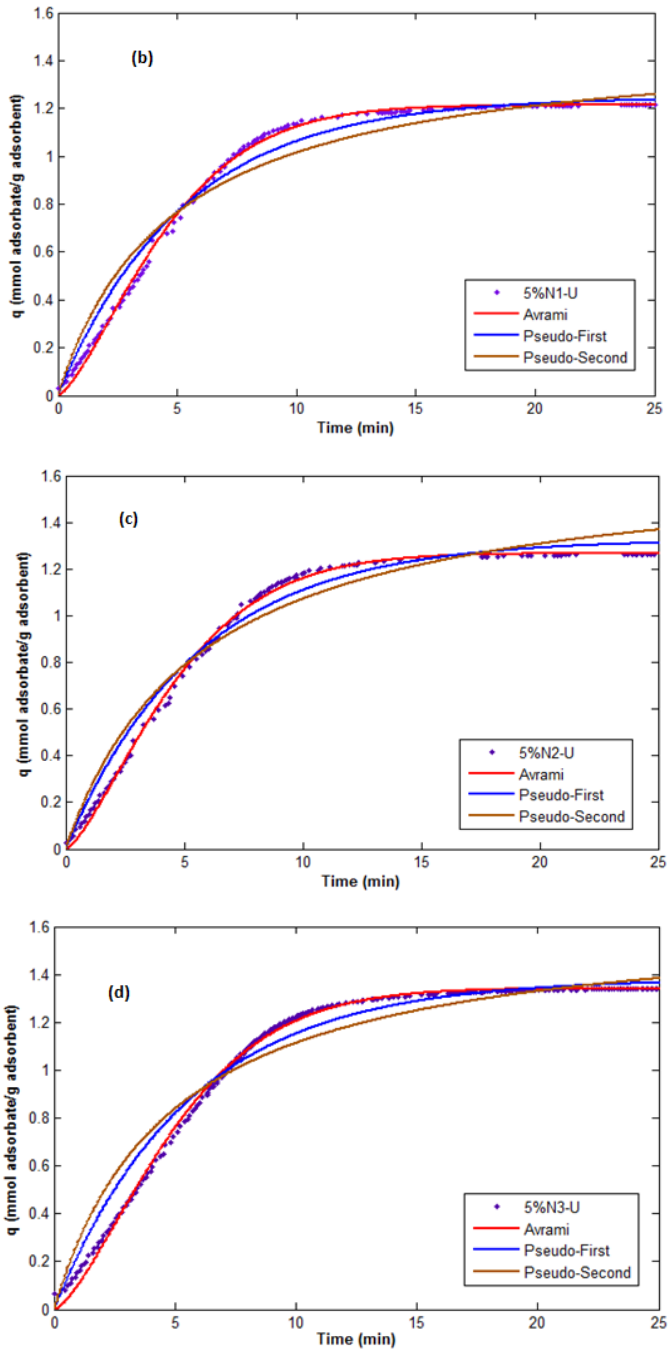

Figure 7: Comparison of kinetic models on experimental CO_2 uptake vs. time for (a) UVM-7, (b) 5%N1-U, (c) 5%N2-U and (d) 5%N3-U

Conclusions

The bimodal siliceous support material has been functionalized with three aminosilanes in order to consider CO_2 capture. These modifications made 6, 10 and 17% increase in their capacity of CO_2 adsorption for mono aminosilane, di aminosilane and tri aminosilane, respectively. Results show a maximum equilibrium capacity of 1.344 mmol CO_2 per g adsorbent for 5%N^3-U with 2.1345 mmol N per g adsorbent, which translated to an amine

efficiency of 0.630 mol CO_2 per mol N. Yoon Nelson model, is in a good agreement with experimental breakthrough curves. Kinetic study of all samples shows that Avrami model with orders of 1.39, 1.40, 1.39 and 1.45 successfully applied for explanation of experimental data obtained from UVM-7, 5%N^1-U, 5%N^2-U and 5%N^3-U, respectively. This can be attributed to the ability of Avrami's model to describe complex adsorption mechanisms because of its fractional order. In addition, the results show pseudo-first model describes the kinetics of adsorption more accurate than pseudo-second model for considered adsorbents.

Nomenclature

q	CO_2 adsorption capacity
F	Total molar flow
$C0$	Concentration of the CO_2 in the feed stream
tq	Adsorption time
W	Amount of the adsorbent
CA	Outlet concentration of the stream
$C0$	Inlet concentration of the stream
qt	Adsorption capacity at a given point in time
qe	Adsorption capacity at equilibrium time
kf	Kinetic constant for pseudo-first order model
ks	Kinetic constant for pseudo-second model,
kA	Kinetic constant for Avrami's kinetic model
n	Order of Avrami model
t	Time elapsed from the beginning of the adsorption process
K	Yoon-Nelson constant
τ	Stoichiometric time (time for $C_A = 0.5\ C_0$),

References:

1- Song, C. (2006). "Global challenges and strategies for control, conversion and utilization of co2 for sustainable development involving energy, catalysis, adsorption and chemical processing." *Catal. Today*, Vol. 115, No. 1–4, pp. 2-32.

2- Aaron, D. and Tsouris, C. (2005). "Separation of co2 from flue gas: A review." *Sep. Sci. Technol.*, Vol. 40, No. 1-3, pp. 321-348.

3- Choi, S., Drese, J.H. and Jones, C.W. (2009). "Adsorbent materials for carbon dioxide capture from large anthropogenic point sources." *Chem Sus Chem*, Vol. 2, No. 9, pp. 796-854.

4- Pachauri, R.K and Reisinger, A. (eds.) (2007).*Climate Change 2007: Synthesis Report*. Contribution of Working Groups I, II and III to the Fourth Assessment Report of the Intergovernmental Panel on Climate Change. IPCC, Geneva, Switzerland.

5- Steeneveldt, R., Berger, B. and Torp, T.A. (2006). "Co2 capture and storage: Closing the knowing–doing gap." *Chem. Eng. Res. Des.*, Vol. 84, No. 9, pp. 739-763.

6- Chu, S. (2009). "Carbon capture and sequestration." *Science*, Vol. 325, No. 5948, pp. 1599-1599.

7- Gough, C. (2008). "State of the art in carbon dioxide capture and storage in the uk: An experts' review." *Int. J. Greenhouse Gas Control*, Vol. 2, No. 1, pp. 155-168.

8- Figueroa, J.D., Fout, T., Plasynski, S., McIlvried, H. and Srivastava, R.D. (2008). "Advances in co2 capture technology—the u.S. Department of energy's carbon sequestration program." *Int. J. Greenhouse Gas Control*, Vol. 2, No. 1, pp. 9-20.

9- Goeppert, A., Czaun, M., Surya Prakash, G.K. and Olah, G.A. (2012). "Air as the renewable carbon source of the future: An overview of co2 capture from the atmosphere." *Energy Environ. Sci.*, Vol. 5, No. 7, pp. 7833-7853.

10- Pennline, H.W., Luebke, D.R., Jones, K.L., Myers, C.R., Morsi, B.I., Heintz, Y.J. and Ilconich, J.B. (2008). "Progress in carbon dioxide capture and separation research for gasification-based power generation point sources." *Fuel Process. Technol.*, Vol. 89, No. 9, pp. 897-907.

11- Sjostrom, S. and Krutka, H. (2010). "Evaluation of solid sorbents as a retrofit technology for co2 capture." *Fuel*, Vol. 89, No. 6, pp. 1298-1306.

12- Ebner, A.D. and Ritter, J.A. (2009). "State-of-the-art adsorption and membrane separation processes for carbon dioxide production from carbon dioxide emitting industries." *Sep. Sci. Technol.*, Vol. 44, No. 6, pp. 1273-1421.

13- Zhao, Y., Ding, H. and Zhong, Q. (2012). "Preparation and characterization of aminated graphite oxide for co2 capture." *Appl. Surf. Sci.*, Vol. 258, No. 10, pp. 4301-4307.

14- Dasgupta, S., Nanoti, A., Gupta, P., Jena, D., Goswami, A.N. and Garg, M.O. (2009). "Carbon di-oxide removal with mesoporous adsorbents in a single column pressure swing adsorber." *Sep. Sci. Technol.*, Vol. 44, No. 16, pp. 3973-3983.
15- Huerta, L., Guillem, C., Latorre, J., Beltrán, A., Martínez-Máñez, R., Marcos, M. D., Beltrán, D., Amorós, P. (2006). "Bases for the synthesis of nanoparticulatedsilicas with bimodal hierarchical porosity." *Solid State Sci.*, Vol. 8, No.8, pp. 940–951.
16- Sayari, A., Belmabkhout, Y. and Serna-Guerrero, R. (2011). "Flue gas treatment via CO_2 adsorption." *Chem. Eng. J.*, Vol. 171, No. 3, pp. 760-774.
17- Serna-Guerrero, R. andSayari, A. (2010). "Modeling adsorption of CO_2 on amine-functionalized mesoporous silica. 2: Kinetics and breakthrough curves." *Chem. Eng. J.*, Vol. 161, No.1-2, pp.182-190.
18- Sing, K. S. W. (1985). "Reporting physisorption data for gas/solid systems with special reference to the determination of surface area and porosity (Recommendations 1984)." *Pure Appl. Chem.*, Vol. 57, No.4, pp. 603-619.
19- Hu, Q., Li, J. J., Hao, Z. P., Li, L. D. andQiao, S. Z. (2009). "Dynamic adsorption of volatile organic compounds on organofunctionalized SBA-15 materials." *Chem. Eng. J.*, Vol. 149, No.1-3, pp. 281-288.
20- Samanta, A., Zhao A., Shimizu, G. K. H., Sarkar, P., and Gupta, R. (2011). "Post-Combustion CO_2 Capture Using Solid Sorbents: A Review." *Ind. Eng. Chem. Res.*, Vol. 51, No.4, pp. 1438-1463.
21- Azizian, S. (2004). "Kinetic models of sorption: a theoretical analysis." *J. Colloid Interface Sci.*, Vol. 276, No.1, pp. 47–52.